HIGH-RESOLUTION LARGE FIELD-OF-VIEW EXPERIMENTAL INVESTIGATION OF TURBULENT CONVECTION VELOCITIES IN A TURBULENT BOUNDARY LAYER

C. Atkinson, N.A. Buchmann, O. Amili, J. Soria
Laboratory for Turbulence Research in Aerospace and Combustion
Department of Mechanical and Aerospace Engineering
Monash University, Clayton Campus
Victoria, Australia, 3800
callum.atkinson@monash.edu

J. Soria
Department of Aeronautical Engineering
King Abdulaziz University, Jeddah, Kingdom of Saudi Arabia

ABSTRACT

Turbulent convection velocities in a turbulent boundary layer at $Re_\theta = 2250$ are examined via the use of a high repetition rate particle image velocimetry measurement undertaken in a water tunnel. Multiple cameras are used to improve the spatial dynamic range of the measurement and reduce the bias towards large-scale structures while simultaneously capturing a wall-normal domain of 0.06δ to 1.7δ. The impact of measurement noise is minimized via careful temporal and spatial filtering of the velocity fields as guided by the comparison of temporal and spatial velocity power spectra with spatially filtered direct numerical simulation data, enabling an estimation of the effective noise-limited spatial and temporal dynamic range of the present experimental measurement. Space-time correlations and phase-spectra are used to estimate the mean and streamwise wave-number dependent convection velocities at various heights above the wall. Results reveal convection velocities greater than the local mean velocity in the lower log layer, decreasing to a level 3.5% lower than the mean velocity in the upper log and wake regions, with smaller convection velocities observed at smaller scales.

INTRODUCTION

Until recently experimental measurements of turbulent flows could generally be divide into either spatially resolved laser diagnostics based measurements [e.g. Particle Image Velocimetry (PIV)] or temporally resolved point measurements [Hot-Wire Anemometry (HWA) or Laser Doppler Anemometry (LDA)]. Typically PIV is limited in temporal resolution due to the firing rate of the laser and the acquisition rate of the cameras, while the finite size and interference between HWA and the number of available LDA systems results in a limited field of view and spatial resolution. As a result of these experimental limitations the spatial structure and wavelengths associated with turbulence measurements are often inferred from temporal data via the application of Taylor's hypothesis (Taylor, 1938) or the frozen turbulence approximation, in which it is assumed that the temporal Eulerian observation of a fixed point in space is approximately the same as the uniform convection of the turbulent flow structure through the same point. Following Townsend (1956) this can be expressed as:

$$U(x,t) = U(x - U_c \cdot \Delta t, t + \Delta t) \tag{1}$$

where Δt is the time separation between two measurements and U_c is the turbulent convection velocity. This convection velocity depends on the propagation of turbulent eddies and is therefore highly relevant to the study of the dynamics of turbulence.

In flows that possess a dominant flow direction and velocity, such as jets, channel flows and boundary layers, the general application of Taylor's hypothesis assumes that the convection velocity is equal to the local mean flow velocity and is independent of frequency or wave-number. While this is generally true when turbulent fluctuations u_i' are small with respect to the U_c, numerous researchers have shown that this approximation breaks-down in regions of strong shear (Lin, 1953) and can lead to the misinterpretation of large-scale structures in jets (Zaman & Hussain, 1981). Recently del Álamo & Jiménez (2009) performed numerical simulations of turbulent channel flows which indicated that while small-scale eddies tend to follow the local mean velocity, large-scale features propagate with a velocity much closer to that of the bulk flow. del Álamo and Jiménez suggest that failure to account for this variation may be partially responsible for the observation of bimodal energy spectra in high Reynolds number wall-bounded flows (Kunkel & Marusic, 2006).

Following Wills (1964) convection velocities can be determined for each Fourier mode as a function of the height above the wall y and the wave-numbers k_x, k_z. However, this requires knowledge of the frequency-wavenumber spectrum $\phi(k_x, k_z, \omega)$ or it's Fourier transform the space-time correlation function. Both of these are difficult to obtain experimentally, however recent advancements in high-

Table 1. Field of view and spatial and temporal resolution of the boundary layer measurements for the investigation of the turbulent convection velocity. Resolution is quoted in terms of the PIV interrogation region size $\Delta W_{x,y}$, light sheet thickness ΔW_z and interframe time Δt which dictate the spatial filtering of PIV. † Interrogation window depth based on assumed laser-sheet thickness of 1 mm.

Researchers	Plane	Cameras	Field of view (x,y,z)	Resolution $\Delta W_x, \Delta W_y, \Delta W_z, \Delta t$
Dennis & Nickels (2008)	longitudinal,	1	$6\delta, -, 3\delta$	0.1δ
$Re_\theta = 4,685$	span-wise plane $(x-z)$			
LeHew *et al.* (2011)	longitudinal,	2	$10\delta, -, 5\delta$	0.16δ
$Re_\theta = 1,280$	span-wise plane $(x-z)$		$4,712^+, -, 2,356^+$	$74^+, 34^+, 74^+, 0.5^+$
de Kat *et al.* (2012)	longitudinal,	2	$2\delta, 0.5\delta, -$	0.007δ
$Re_\tau = 2,700$	wall-normal plane $(x-y)$		$5400^+, 1350^+, -$	$20^+, 20^+, 27^{+\dagger}, 1.5^+$
Present	longitudinal,	2	$3.2\delta, 1.7\delta, -$	0.03δ
$Re_\theta = 2,250$	wall-normal plane $(x-y)$		$2680^+, 1424^+, -$	$23^+, 23^+, 23^+, 0.3^+$

speed digital imaging and the availability of high-speed lasers have seen a renewed interest in the experimental measurement of turbulent convection velocities. Using time-resolved planar PIV measurements in a water tunnel Dennis & Nickels (2008) were able to estimate a mean convection velocity from the space-time correlation $R_{u'u'}(\Delta x, \Delta t)$ that was only slightly higher than the local mean velocity, however they did not investigate the effect of spatial resolution and the relative convection of different scales. LeHew *et al.* (2011) performed similar measurements using two high-speed camera with a slight overlap in order to increase their field of view and used this data to calculated the 3D power spectra $\Phi(k_x, k_z, \omega)$, enabling the calculation of k_x, k_z dependent convection velocities. At a wall-normal height of $y^+ = 34$ LeHew *et al.* (2011) indicate a convection velocity greater than the local mean and increasing with streamwise wave-number k_x over most scales, as derived from a linear fit to the local maximum in the premultipled 2D $k_x\omega\phi(k_x, \omega)$ spectrum. Following the method of del Álamo & Jiménez (2009) and using the 3D $\Phi(k_x, k_z, \omega)$ spectra LeHew *et al.* (2011) examined the convection velocity in the $k_x - k_z$ plane, which unlike the 2D results indicates that most scales travel slower than the local mean velocity, with the exception of the largest scales $1.2 < k_x\delta < 3$, inline with the results of del Álamo & Jiménez (2009), but counter to those of the 2D spectra. Unfortunately spectra calculated from PIV data can be quite sensitive to measurement noise and the number of velocity vectors over which they are calculated. de Kat *et al.* (2012) investigated the influence of spatial and temporal resolution on the experimental investigation of turbulent convection velocity and indicate that the use of a phase-spectrum or the phase of the cross-spectrum between PIV data at times t and $t + \Delta t$ can provided better estimates of the k_x dependent convection velocity than methods based on the calculation of the 2D $\phi(k_x, \omega)$ spectrum.

In this paper the convection velocities of a turbulent boundary layer are investigated using high repetition rate PIV measurements (HR-PIV) undertaken in a large horizontal water tunnel with a high temporal and spatial resolution, in order to reduce the bias towards the convection velocity of the large-scale structures. The noise-limited spatial and temporal dynamic range of the present measurement is estimated via the comparison of the measured spatial and temporal velocity power spectra with those of spatial filtered direct numerical simulation data. Filtering is applied to limit the influence of measurement noise, following which convection velocities are estimated using both the space-time correlation approach followed by Dennis & Nickels (2008) and the phase-spectrum approach of de Kat *et al.* (2012).

EXPERIMENTAL SETUP

Experiments were performed in a longitudinal, wall-normal $(x - y)$ plane spanning the log and wake layers of a turbulent boundary layer, formed on the floor of the 0.5×0.5 m cross-section horizontal water tunnel at the Laboratory for Turbulence Research in Aerospace and Combustion at Monash University. The boundary layer was tripped at the outlet of the contraction using a cylindrical rod with the addition of a trailing sandpaper element as discussed in Herpin *et al.* (2008). HR-PIV measurements were performed approximately 4 m downstream of the trip, resulting in a boundary layer approximately 38.6 mm high with a momentum thickness based Reynolds number of $Re_\theta = 2,250$.

To reduce the influence of limited spatial resolution and spatial record lengths, experiments were performed using two high-speed PCO. DiMax CMOS cameras (2016×2016 pixel each), aligned with a small overlap in the longitudinal direction. Illumination was provided by the use of a 60 mJ Quantronix Darwin Duo Nd:YLF laser collimated into a 1 mm light sheet at a recording rate of 1.25 kHz. The flow was seeded with Potters hollow glass spheres with a mean diameter of 11 μm and a specific gravity of 1.1. The combination of long-time scales in water and the use of multiple cameras provides both a high-temporal and high-spatial resolution measurement. The field of view and spatial resolution associated with this measurement are summarized in table 1 and indicate a significantly higher resolution Dennis & Nickels (2008) and LeHew *et al.* (2011) and higher temporal resolution than de Kat *et al.* (2012).

Velocity fields were processed using a multigrid PIV algorithm (Soria, 1996) with window deformation (Huang *et al.*, 1993; Scarano, 2002) and an initial and final interro-

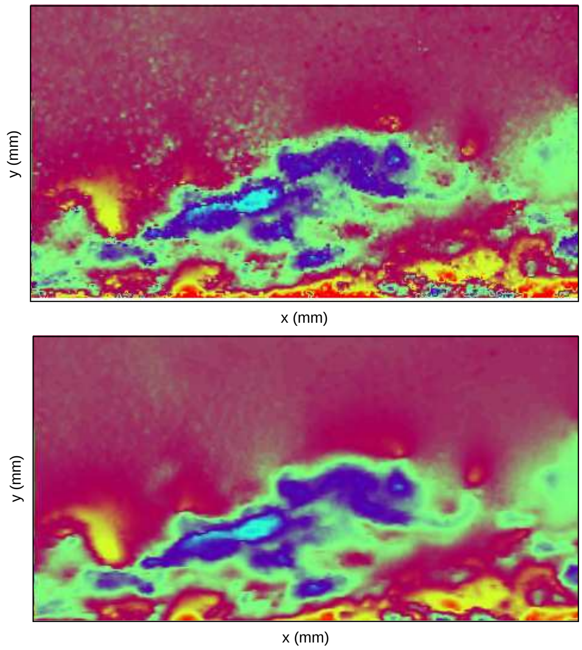

Figure 1. Instantaneous iso-contours of the streamwise velocity fluctuations in the HR-PIV measurements of a turbulent boundary layer after merging velocity fields: (*top*) raw velocity field data; (*bottom*) temporally and spatially filtered velocity field.

gation window size of 64×64 and 32×32 pixels, respectively. A window overlap of 50% was applied to the final pass. Vector validation was performed using normalized median vector validation (Westerweel & Scarano, 2005) in both space and time while rejected vectors were interpolated using a local temporal and spatial mean. Five sets of 6305 vector fields were recorded in each camera. Velocity fields were merged in the streamwise direction by imposing a sharp transition in the middle of the overlap region, after dewarping the velocity fields from each camera using a standard polynomial calibration (Soloff *et al.*, 1997). Further parameters associated with the PIV analysis are given in Table 2. An example of an instantaneous merged field is shown in figure 1 with mean and fluctuating velocity profiles shown in figure 2 before and after noise filtering as discussed in the following section.

Table 2. Parameters of the HR-PIV boundary layer measurements

boundary layer thickness	$\delta^+ = 840$
Friction velocity	$u_\tau = 0.018$ ms^{-1}
Magnification	0.33
Spatial resolution	30.0 pixels/mm
Lens aperture	$f_\# = 4$
Particle image diameter	$d_p \approx 1$ pixel
Depth of field	$\Delta z \approx 0.7$ mm
Light-sheet thickness	$\Delta z = 1$ mm

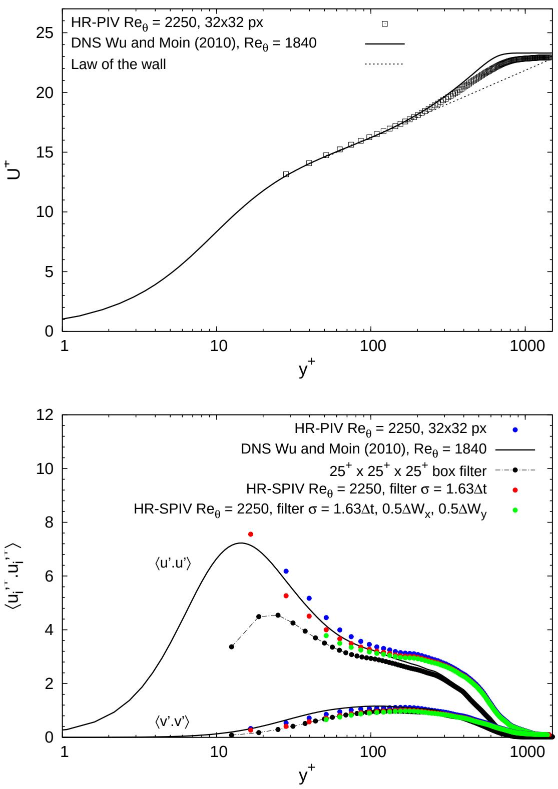

Figure 2. Mean and wall-normal velocity and Reynolds stress profiles for the HR-PIV measurements of a turbulent boundary layer.

DETERMINING THE NOISE-LIMITED DYNAMIC RANGE OF THE EXPERIMENT

HR-PIV is capable of providing experimental measurements of both the spatial and temporal evolution of a turbulent flow, however it is important to recognize the limitations on both the spatial and temporal dynamic range of such measurements. In theory the spatial dynamic range of PIV measurements are limited by the field of view and the interrogation window size $\Delta W_x, \Delta W_y$ and the light sheet thickness (in this case denoted as the effective interrogation window size in the spanwise direction ΔW_z), while the temporal dynamic range is similarly limited by the number of images that can be recorded by the camera and the maximum recording rate or inter-frame times Δt of both the cameras and laser. However, in practice the presence of PIV measurement noise means that the smallest scales that can be accurately resolved by a given PIV measurement are generally significantly larger than cut-off associated with the chosen interrogation window size or inter-frame time (Foucaut *et al.*, 2004). This introduces an effective noise limited cut-off in both the spatial and temporal spectra, beyond which the true turbulent signal cannot be distinguished from the measurement noise. As discussed in Atkinson *et al.* (2013) this measurement noise is often masked by the spatial filtering of PIV such that the influence of measurement noise is often underestimated.

In order to reduce the influence of measurement noise on the estimation of the convection velocity and to quantify the effective noise-limited spatial and temporal dynamic range, the temporal and spatial longitudinal velocity power spectra are examined after treating the data for periodicity as discussed in (Foucaut *et al.*, 2004) with tem-

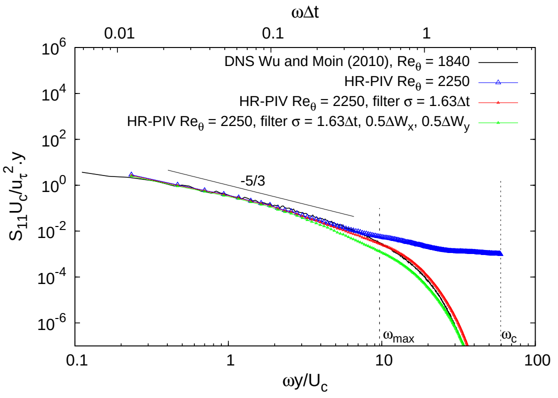

Figure 3. Temporal velocity power spectra at $y^+ = 100$ for HR-PIV measurements of a turbulent boundary layer at $\mathrm{Re}_\theta = 2{,}250$ and DNS of Wu & Moin (2010) at $\mathrm{Re}_\theta = 1840$. Temporal spectra is calculated over a domain of only $240\Delta t$. U_c is the convection velocity assumed to be equal to the local mean velocity.

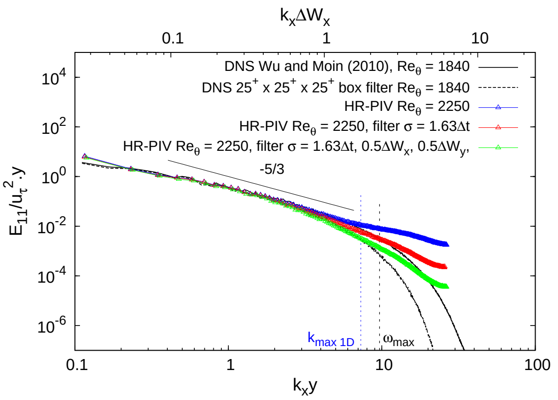

Figure 4. Spatial velocity power spectra at $y^+ = 100$ for HR-PIV measurements of a turbulent boundary layer at $\mathrm{Re}_\theta = 2{,}250$ and DNS of Wu & Moin (2010) at $\mathrm{Re}_\theta = 1840$.

poral spectral calculated over a range of $240\Delta t$. Figure 3 shows the clear influence of white measurement noise on the temporal spectra of the unfiltered HR-PIV spectra taken at $y^+ = 100$. In the absence of temporal DNS spectra at the same spatial resolution as the PIV, the noise-limited temporal frequency $\omega_{\max}$ was determined following Foucaut *et al.* (2004) where $\omega_{\max}$ is defined as the frequency at which the signal to noise ratio SNR = 1, $S_{11\,PIV}$ is the spectra obtained from PIV and $S_{11\,flow}$ is the true spectra of the flow, or in this case the spectra obtained from the DNS:

$$S_{11\,PIV}(\omega_{\max}) = 2S_{11\,flow}(\omega_{\max})\left(\frac{\sin\omega_{\max}\Delta t/2}{\omega_{\max}\Delta t/2}\right)^2 \tag{2}$$

In order to reduce the influence of measurement noise at frequencies greater than $\omega_{\max}$ the HR-PIV velocity field were spatially filtered with using an 11 point Gaussian kernel in the temporal domain with $\sigma_t = 1.63\Delta t$, which provides a -3 dB cut-off at $\omega_{\max}\Delta t \approx 0.51$.

Figure 4 shows the influence of temporal filtering on the spatial velocity power spectra, which while now similar to the raw DNS spectra, still peals away from the DNS

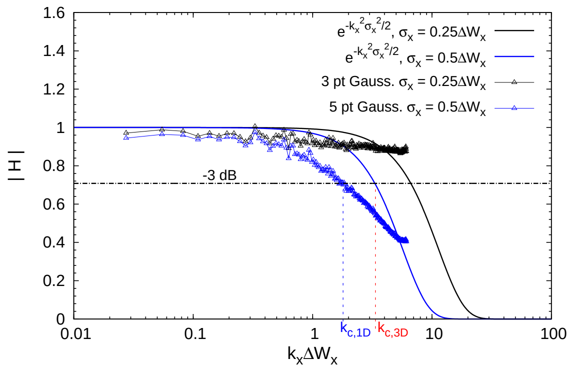

Figure 5. Apparent 1D transfer function associated with the 2D Gaussian filtering of HR-PIV data of a turbulent boundary layer at $\mathrm{Re}_\theta = 2{,}250$ at y+ = 100.

spectra if the DNS is box filtered with interrogation window dimensions similar to that of the present PIV measure. The dashed spectra represents the spectra that should be provide by the HR-PIV measurement in the absence of measurement noise, the calculation and details of which are explained in Atkinson *et al.* (2013). Following the methodology in Atkinson *et al.* (2013), which accounts for the true 1D transfer function of PIV $H(k_x)$, the noise-limited wavenumber $k_{\max}$ can be determined as:

$$\begin{aligned} E_{11\,PIV}(k_{\max\,1\mathrm{D}}) &= 2E_{11\,flow}(k_{\max\,1\mathrm{D}})\left|H(k_{\max\,1\mathrm{D}})\right|^2 \\ &\approx 2E_{11\,filt}(k_{\max\,1\mathrm{D}}) \end{aligned} \tag{3}$$

where $E_{11\,filt}(k_x)$ is the spectrum of the DNS after filtering at the resolution of the PIV. In this case 2D Gaussian filtering in the x and y directions with a five point kernel and $\sigma_{x,y} = 0.5\Delta W_{x,y}$ provide a -3 dB cut-off at $k_{\max\,1\mathrm{D}}\Delta W_x \approx 1.73$ in the 1D spectra. Owing to the 1D representation of a 2D filter this cut-off corresponds to a 3D cut-off of $k_{\max}\Delta W_x \approx 3.36$. This is due to the difference in the true 2D and apparent 1D transfer functions of the filter as shown in figure 5. A detailed explanation of this behavior is given in Atkinson *et al.* (2013).

The effect of the combined temporal and spatial filtering can be observed in both the iso-contours of the instantaneous velocity field (see figure 1) and the Reynolds stress-profiles (see figure 2), where filtering reduces the fluctuations to a level more inline with those of the noise-free spatially filtered DNS. The theoretical and noise-limited temporal and one-dimensional spatial dynamic range of the measurements are given in table 3. Assuming the the noise-level in the spectra is independent of wall-height the relative noise-limited wave-numbers will decrease with height above the wall as the energy level in the turbulent fluctuations is reduced, relative to a constant background noise. Figure 6 shows the effective noise limited waves-numbers as a function of wall-height, based on the energy level of the noise identified at $y^+ = 100$.

SPACE-TIME CORRELATION DERIVED CONVECTION VELOCITY

The space-time correlations associated with the filtered HR-PIV data were obtained by obtaining the correlation of

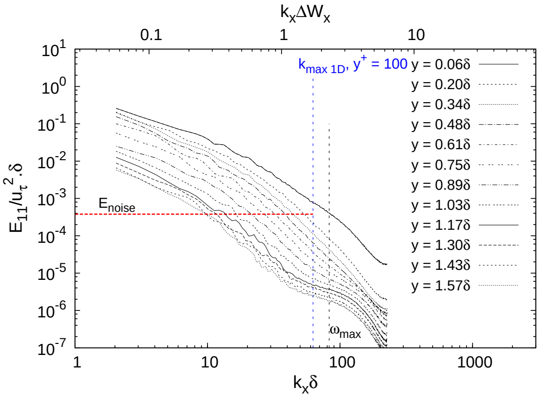

Figure 6. Noise-limted wave-number at different wall heights in the HR-PIV data of a turbulent boundary layer at $\mathrm{Re}_\theta = 2,250$ relative to the spectral energy content of the measurements noise at $y^+ = 100$.

streamwise or wall-normal velocity components with relative offsets in the streamwise Δx and temporal Δt directions:

$$R_{u'u'}(\Delta x, y, \Delta t) = \frac{\langle u'(x,y,t) \cdot u'(x+\Delta x, y, t+\Delta t)\rangle}{\sigma'_u(y) \cdot \sigma'_u(y)} \tag{4}$$

where u' denotes the fluctuating velocity component. As in the approach of Dennis & Nickels (2008) the convection velocity was obtained by fitting a line to the maximum in the space-time correlation, which represents the mean convection velocity for all resolved scales, maintaning the maximum correlation between the spatially and temporally spaced fluctuations.

Figure 7 shows an example of a space-time correlation field at $y/\delta \approx 0.2$ or $y^+ \approx 170$, indicating that a streamwise velocity fluctuations on average maintains a correlation coefficient $R_{u'u'} > 0.6$ over a distance of almost 2δ at this height. In order to determine the mean convection velocity at various wall heights a 3 points Gaussian fit, similar to that used in PIV, was used to determine the peak in the correlation map as a function of Δx. A linear fit was then performed to determine the gradient of the peak, as indicated by the black line in Figure 7.

The variation in the mean convection velocity $\langle U_c \rangle$ with wall height is shown by figure 8. Results indicate convection velocities greater than the local mean velocity for wall heights $y^+ < 300$ or $y < 0.35\delta$, similar to those observed by del Álamo & Jiménez (2009) in turbulent channel flows when only the large-scale Fourier modes are considered. Higher convection velocities for the wall-normal v' fluctuations near the wall and lower velocities relative to

Table 3. Temporal and spatial dynamic range of the HR-PIV boundary layer measurements at $y^+ = 100$.

Domain		Theoretical	Noise-limited
Spatial	$k_x \Delta W_x$	$0.056 - 3.1$	$0.056 - 1.7$
	$k_x \nu / u_\tau$	$0.002 - 0.14$	$0.002 - 0.075$
Temporal	$\omega \Delta t$	$0.001 - 3.1$	$0.001 - 0.51$
	$\omega \nu / u_\tau^2$	$0.003 - 10$	$0.003 - 1.7$

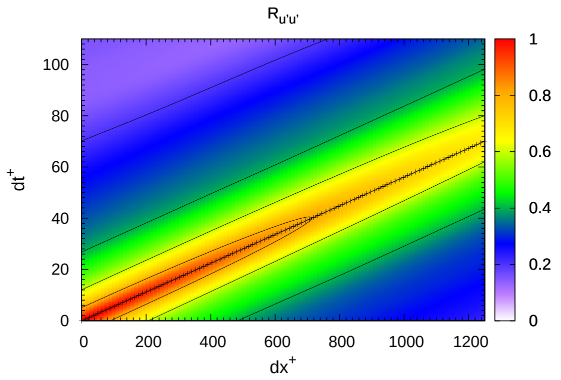

Figure 7. Space-time correlation at $y+ = 170$ calcualted from HR-PIV data of a turbulent boundary layer at $\mathrm{Re}_\theta = 2,250$.

the u' fluctuation at the top of the boundary layer are also consistent with the time-resolved channel flow DNS results. Within the spatial resolution limits of the present experiment the average convection velocity across the resolved scales is shown to vary from the local mean by up to 3.5% in the wake region. Interestingly the u' fluctuations convect at velocities lower than the free-stream velocity upto a height of approximately 1.5δ, which is consistent with fluctuations in the position of the turbulent / non-turbulent interface. This lag persists beyond $y = 1.6\delta$ for the wall-normal fluctuations.

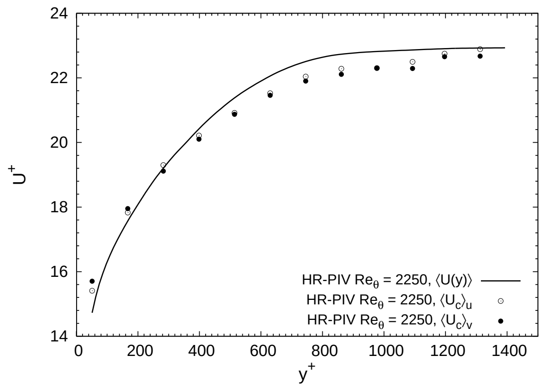

Figure 8. Mean convection velocity at various heights above the wall as calcualted from space-time correlation of the HR-PIV data of a turbulent boundary layer at $\mathrm{Re}_\theta = 2,250$. Convection velocities are calculated from the space-time correlations of u' and v'. Local mean velocity is shown for comparison.

PHASE SPECTRUM DERIVED CONVECTION VELOCITIES

In order to examine the variation in convection velocity as a function of streamwise wave-number k_x, de Kat *et al.* (2012) advocates the use of the phase-spectrum or the phase angle of the cross-spectra between velocity fluctuations at times t and $t+\Delta t$ where:

$$u_c(k_x,y,t) = \frac{\langle \Psi(k_x,y,t)\rangle}{k_x \cdot \Delta t} \qquad (5)$$

Their results suggest that this method is less susceptible to noise and limited fields of view which can effect the calculation of the 2D $\phi(k_x,\omega)$ spectrum.

Figure 9 shows the convection velocity at different heights above the wall as a function of the streamwise wavenumber k_x with the convection velocity normalized by the local mean velocity at each height. In order to limit the influence of the measurement noise the phase-spectra at each height were truncated where the energy in the spectra decreases to a SNR of unity with respect to the noise level as depicted by the line in figure 6. Results indicate higher convection velocities for the large-scale motions at all heights, similar to the channel flow DNS of del Álamo & Jiménez (2009), over the same range of wall heights and scales. This is in direct contrast to the results of LeHew *et al.* (2011) based on fitting to the 2D $\phi(k_x,\omega)$ spectrum, which suggests the benefits of the present approach.

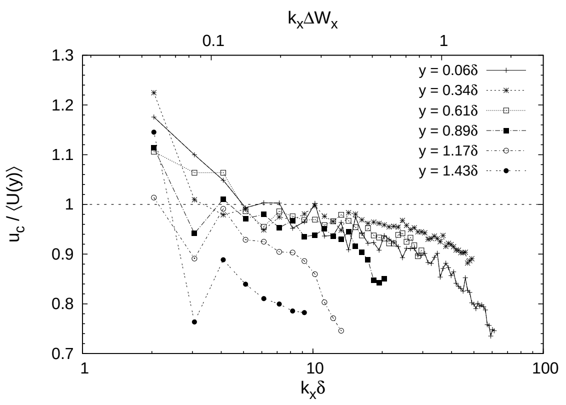

Figure 9. Convection velocity at various heights above the wall as calculated from the phase-specta the HR-PIV data at times t and $t+\Delta t$. Convection velocities are calculated for the streamwise u' fluctuations and normalized by the local mean velocity.

CONCLUSION

Experiments were performed in a water tunnel using high repetition rate PIV in order to investigate the convection velocities in a turbulent boundary over a wall-normal range of 0.06δ to 1.6δ. Multiple cameras were used to improve the spatial dynamic range of the measurement and reduce the bias towards large-scale structures. To restrict the influence of measurement noise and quantify the effective noise-limited spatial and temporal dynamic range of the measurement an extensive validation was performed via comparison with spatial filtered DNS data. Space-time correlations indicate mean convection velocities greater than the local mean velocity for wall heights $y^+ < 300$ or $y < 0.35\delta$ and up to 3.5% lower than the mean velocity in the wake region. Phase-spectra show decreasing convection velocity at higher wave-numbers, which are mostly consistent with results from DNS of turbulent channel flows.

ACKNOWLEDGMENTS

The support of Australian Research Council for this work is gratefully acknowledged.

REFERENCES

del Álamo, J. C. & Jiménez, J. 2009 Estimation of turbulent convection velocities and corrections to taylor's approximation. *J. Fluid Mech.* **640**, 5–26.

Atkinson, C., Buchmann, N. A., Amili, O. & Soria, J. 2013 On the appropriate filtering of piv measurements of turbulent shear flows. *Experiments in Fluids* **submitted**.

Dennis, D. J. C. & Nickels, T. B. 2008 On the limitations of taylor's hypothesis in constructing long structures in a turbulent boundary layer. *J. Fluid Mech.* **614**, 197–206.

Foucaut, J. M., Carlier, J. & Stanislas, M. 2004 PIV optimization for the study of turbulent flow using spectral analysis. *Measurement Science and Technology* **15**, 1046–1058.

Herpin, S., Wong, C. Y., Stanislas, M. & Soria, J. 2008 Stereoscopic piv measurements of a turbulent boundary layer with a large spatial dynamic range. *Exp Fluids* **45**, 745–763.

Huang, H. T., Fiedler, H. E. & Wang, J. J. 1993 Limitations and improvements of PIV; part II: particle image distortion, a novel technique. *Experiments in Fluids* **15**, 263–273.

de Kat, R., Gan, L., Dawson, J. R. & Ganapathisubramani, B. 2012 Limitations of estimating turbulent convection velocities from PIV. In *16th Int. Symp. App. Laser Techniques to Fluid Mech.*. Lisbon, Portugal, 9-12 July.

Kunkel, G. J. & Marusic, I. 2006 Study of the near-wall-turbulent region of the high-reynolds-number boundary layer using atmospheric data. *J. Fluid Mech.* **548**, 375–402.

LeHew, J., Guala, M. & McKeon, B. J. 2011 A study of the three-dimensional spectral energy distribution in a zero pressure gradient turbulent boundary layer. *Exp Fluids* **51**, 997–1012.

Lin, C. C. 1953 On taylor's hypothesis and the acceleration terms in the navier-stokes equations. *Q. Appl. Math.* **10** (4), 295–306.

Scarano, F. 2002 Iterative image deformation methods in PIV. *Measurement Science and Technology* **13** (R1-R19).

Soloff, S. M., Adrian, R. J. & Liu, Z.-C. 1997 Distortion compensation for generalized stereoscopic particle image velocimetry. *Measurement Science and Technology* **8**, 144–1454.

Soria, J. 1996 An investigation of the near wake of a circular cylinder using a video-based digital cross-correlation particle image velocimetry technique. *Experimental Thermal Fluid Science* **12**, 221233.

Taylor, G. I. 1938 The spectrum of turbulence. *Proc. R. Soc. Lond.* **164** (919), 476–490.

Townsend, A. A. 1956 *The Structure of Turbulent Shear Flows*. UK: Cambridge University Press.

Westerweel, J. & Scarano, F. 2005 Universal outlier detection for PIV data. *Experiments in Fluids* **39**, 1096–1100.

Wills, J. A. B. 1964 Convection velocities in turbulent shear flows. *J. Fluid Mech.* **20**, 417–432.

Wu, X. & Moin, P. 2010 Transitional and turbulent boundary layer with heat transfer. *Phys. Fluids* **22**.

Zaman, K. B. M. Q. & Hussain, A. K. M. F. 1981 Taylor hypothesis and large-scale coherent structures. *J. Fluid Mech.* **112**, 379–396.